33rd Symposium on Naval Hydrodynamics
Osaka, Japan, 18-23 October 2020

Effect of Non-Condensable Gas on the Thermophysical Properties of Bubbly Water and on Bubble Collapse Dynamics Probed by Molecular Simulations

J. Ilja Siepmann*, Jingyi L. Chen, Buyun Liang, and Krishnan Mahesh
(University of Minnesota, USA)
*Corresponding author, E-mail: siepmann@umn.edu

ABSTRACT

Numerical results and visualizations for equilibrium properties of bubbly water and for bubble collapse dynamics obtained from Monte Carlo and molecular dynamics simulations for coarse-grained water and nitrogen models are presented and discussed to elucidate the effects of nitrogen and to provide insights for improving the underlying physical assumptions used in computational fluid dynamics studies of multi-phase flow.

With regard to equilibrium properties, our simulations indicate that, at room temperature, the solubility of nitrogen increases significantly as water is placed under tension (i.e., homogeneously stretched water), but that the effects of nitrogen on bubble volume fraction and bubble stability are relatively small.

Molecular dynamics simulations for the collapse of a vapor bubble indicate that very large system sizes ($> 10^7$ molecules) are needed to reach convergent behavior. Here, supersonic speeds for the decrease of the bubble radius are reached preceding the initial bubble collapse. Concomitantly, extreme local heating with temperatures exceeding 2000 K for more than 1% of the molecules at the center of the collapsing bubble is observed. After initial collapse, the bubble rebounds and a high-density wave propagates outward at supersonic speeds.

The presence of nitrogen (at a mole fraction of 1.2×10^{-5} corresponding to the amount of nitrogen in aqueous solution at 298 K and a vapor pressure of 1 bar) leads to a slight increase in the bubble collapse time and reduction in the speed for the decrease of the bubble radius before collapse, but the rebound is more pronounced.

INTRODUCTION

Understanding and predicting multi-phase flows is inherently challenging due to the variety of phenomena involved, that can span large temporal and spatial scales. Currently, computational fluid dynamics (CFD) simulations of multi-phase flows include many of these phenomena only through empirically motivated source/drain terms and rely on bulk properties of the multiple phases. Thus, much ongoing research is devoted to improving the underlying physical models and eliminating empiricism in CFD simulations (Crowe, 2005; Yadigaroglu & Hewitt, 2017). In contrast, molecular simulations directly apply statistical mechanics or classical mechanics to generate trajectories of molecular (particle) systems, where the particle interactions are computed either directly from quantum mechanics or are represented through force fields. Although molecular simulations can only access much smaller temporal and spatial scales compared to CFD approaches, the data from these simulations can be very useful because of the explicit consideration of the molecular nature of fluids and the ability to probe finite-size model system under conditions that are not stable for bulk systems. This allows for molecular simulations to assess some of the underlying equations applied in CFD for predicting cavitating multi-phase flow. Since molecular dynamics simulations do not make assumptions about the equation of state nor transport coefficients (as would be required for solving the Navier-Stokes hydrodynamics equations) and explicitly account for interfacial effects, these simulations are especially appropriate for modeling the final stages of bubble collapse.

The objectives of this study are twofold: (i) to provide data for the solubility of nitrogen in

homogeneously stretched liquid water phases and for the influence of nitrogen on the thermophysical properties of homogeneously stretched and bubbly water phases; and (ii) to provide microscopic-level information on the bubble collapse process for neat water and water-nitrogen systems.

Experimental data for the nitrogen solubility are available at temperatures ranging from 274 to 658 K and pressures from 45 kPa to 262 MPa (Rettich, *et al.*, 1984; Japas & Franck, 1985). Near ambient conditions, nitrogen is only sparingly soluble in water with an equilibrium mole fraction of 1.2×10^{-5} for the binary water-nitrogen mixture at $T = 298$ K and $P = 0.1$ MPa (Rettich, *et al.*, 1984). For pressures up to 10 MPa, the solubility is well described by Henry's law (Chapoy, *et al.*, 2004), and the Henry's law coefficient increases nearly linearly and approximately doubles from 273 to 323 K (Rettich, *et al.*, 1984). However, there is a data gap on the nitrogen solubility in (metastable) liquid water under tension, i.e., conditions that can be present in cavitating multi-phase flows. Thus, additional data is needed to understand the effects of nitrogen on the thermophysical properties of water under tension. Here, Monte Carlo simulations allowing only for the transfer of nitrogen molecules are used to determine the nitrogen solubility in homogeneously stretched water phases.

Molecular dynamics simulations have been used previously to provide molecular-level information for the collapse of nanobubbles. Early simulations were limited to relatively small systems consisting of 10^5 Lennard-Jones particles (Matsumoto, *et al.*, 2000; Xiao, *et al.*, 2002) but, more recently, system sizes of 10^7 Lennard-Jones particles have been utilized (Holyst, *et al.*, 2010). Here, we report molecular dynamics simulations for slightly larger systems (up to 7×10^7 particles) using coarse-grained models designed to represent water and nitrogen molecules, and for smaller systems (up to 9×10^6 particles) using atomistic models.

MODELS AND SIMULATION DETAILS

Force Fields

For computational efficiency, the coarse-grained mW model is utilized for water (Molinero & Moore, 2009). This model represents water by a single site but includes, in addition to a 2-body distance-dependent potential, also a 3-body interaction based on the two distances and the angle of a triad to favor tetrahedral structuring. The water-water interactions for the mW model are very short-ranged and approach zero at a distance of 0.43065 nm (i.e., about 1.5 times the hydrogen-bond distance). For this work, we developed a single-site nitrogen model compatible with the mW model. Nitrogen-nitrogen and nitrogen-water interactions are described by shifted-force Lennard-Jones interactions with a truncation distance of 0.9 nm, and well depth and size parameters fitted to reproduce the critical point of nitrogen and its solubility in water.

Simulation Details

Isobaric-isothermal Gibbs ensemble Monte Carlo simulations (Panagiotopoulos, *et al.,* 1988) were carried out to determine the nitrogen solubility at $T = 298$ K and $P_{\text{total}} = 1$ atm for a system consisting of 2000 water and 200 nitrogen molecules. Gibbs ensemble simulations using a pseudo-osmotic (adsorption) set-up, where the volume and number of water molecules were fixed for the aqueous phase, were carried out for homogeneously stretched water systems at $T = 298$ K, $P_{\text{nitrogen}} = 1$ atm, and specific water densities, D_w, ranging from 940 to 990 kg/m^3 (with a box lengths of 4 nm and 2010, 2032, 2053, 2074, 2095, and 2117 water molecules). At least 50000 Monte Carlo cycles (MCCs, where a cycle consists of $N_{\text{total}} = N_{\text{water}} + N_{\text{nitrogen}}$ moves) were used for equilibration, and the production periods consisted of 100000 MCCs. Statistical uncertainties were estimated from the production periods of eight independent simulations and are reported here as the standard error of the mean at 95% confidence interval.

To determine the equilibrium thermo-physical properties of homogeneously stretched and bubbly (water + nitrogen) phases, molecular dynamics simulations in the canonical (N_{water}, N_{nitrogen}, V, T) ensemble were carried at $T = 298$ K and a system volume of 512 nm^3 (box length of $L = 8$ nm). Here, the simulations span the same range for the specific water density from 800 to 998 kg/m^3 as was investigated in prior work on neat water (Chen, *et al.,* 2019). These systems contain from 13688 to 17075 water molecules. For this size, a saturated liquid phase would contain on average only 0.2 nitrogen molecules. Thus, the current simulations used a mole fraction of about 10^{-3} (80 times higher than the equilibrium mole fraction at $P = 0.1$ MPa), i.e., from 14 to 17 nitrogen molecules. Due to the nucleation free energy barrier for the formation of a bubble, these systems show a pronounced hysteresis loop (Chen, *et al.,* 2019). Thus, three simulation protocols were utilized to explore the homogeneously stretched region above the binodal point, the metastable homogeneously stretched region between spinodal and binodal points, and the bubbly region. For

protocol H, a homogeneous configuration was used as the starting point. For protocols BI and BO, an initial heterogeneous configuration was generated with all water molecules placed outside of a sphere with its center located at the center of the simulation box (Chen, *et al*., 2019), but the nitrogen molecules are placed either all inside this sphere (protocol BI) or outside of this sphere (protocol BO). For densities below the binodal point, protocols BI and BO should reach the same equilibrium state after the nitrogen molecules have distributed themselves between the bubble and liquid regions. The equilibrium periods consisted of at least 120 ns, followed by production periods of 20 ns. Statistical uncertainties were estimated from the standard error of the mean at 95% confidence interval obtained from the production periods of five independent simulations.

Using a set-up with a pre-formed void or gas bubble in a sub-region of the system, molecular dynamics simulations in the microcanonical (N_{water}, N_{nitrogen}, V, E) ensemble were used to probe bubble collapse. For all systems with the mW model studied in this work, the specific water density was set at 998 kg/m^3, i.e., just above the saturated density of 997.66 kg/m^3 for the mW model at 298 K (Chen, *et al*., 2019). Four system sizes with L = 16, 32, 64, and 128 nm were used with the number of water molecules ranging from 136647 to 69963308. The simulation box is initially divided into bubble and liquid regions by a spherical wall at radius R_{I} placed at the center of cubic simulation box, and the R_{I} / L ratio was set to 0.15 for all four sizes. For the largest system (L = 128 nm), a separate simulation with an additional 832 nitrogen molecules (i.e., corresponding to a mole fraction of 1.2 × 10^{-5}) was also carried out to investigate the effect of a "non-condensable" gas on the bubble collapse. For the second-largest system (L = 64 nm), a separate simulation for the TIP4P/2005 water model [Abascal & Vega, 2005] with an overall density of 995 kg/m^3 and R_{I} / L = 0.15 was also carried out to explore sensitivity to the underlying force field used for the simulations.

The procedure for simulating the vapor or gas bubble collapse was divided into three stages. First, the liquid water region was equilibrated in the canonical ensemble at T = 298 K. Due to the low saturated vapor pressure of water, all of the water molecules were placed outside the spherical wall. (It should be noted that both water models under predict the vapor pressure (Chen, *et al*., 2019).) Thus, the initial water density in the liquid region is about 1010 kg/m^3, and the density of the liquid region decreases with decreasing bubble volume. For the investigation of the gas bubble collapse, all nitrogen molecules were initially placed inside the spherical cavity. Neither water nor nitrogen molecules were allowed to pass through the spherical wall. The pre-equilibration stage is run for at least 250 ps. Next, the wall was removed and the systems were allowed to undergo a short relaxation period of 0.1 ps, during which the center of mass momentum of the simulation box is removed. Finally, the simulations were switched to the microcanonical ensemble, and the timer for bubble collapse process was started. For the mW model, a time step of 5 fs was used for the equilibration and relaxation periods and also for about 95% of the bubble collapse process. However, the time step was reduced to 2.5 fs for the final part of the collapse process to ensure satisfactory energy conservation during this more violent part. For the TIP4P/2005, a time step of 1 fs was used throughout the trajectory.

The data for the (water + nitrogen) mixtures are compared to data from a previous study that considered the properties of neat water phases (Chen, *et al.,* 2019). Figure 1 shows some of the most important data obtained for the mW model and L = 8 nm (approximately 10^4 water molecules). Large negative pressures are observed for the homogeneously stretched and bubbly phases that for the latter region agree well with predictions from the Young-Laplace equation.

For all simulations, the instantaneous region belonging to the bubble was determined considering only the location of water molecules with the approach described by Chen, *et al*. (2019); that is a mesh size of 0.2 × 0.2 × 0.2 nm^3 was used and the sum of the meshes belonging to the largest cluster determine its volume. Since all bubbles show very low shape anisotropy, the bubble radius is calculated from the volume assuming a spherical shape, and many properties can be analyzed as radial profiles.

RESULTS

Nitrogen Solubility in Water under Tension

Chen, *et al*. (2019) found a value of 930 kg/m^3 for the spinodal density of neat water described by the mW model using L = 4 nm. Given the low equilibrium mole fraction of 1.2 × 10^{-5} for the binary water-nitrogen mixture at T = 298 K and P = 0.1 MPa (that is reproduced by the single-site nitrogen model compatible with the mW water model), the water densities investigated here (D_{w} ranging from 940 to 990 kg/m^3 for L = 4 nm) yield homogeneously stretched phases. It should be noted that the average number of nitrogen molecules present in these stretched liquid phases is less than 0.2 for all D_{w} values, i.e., the perturbation on the water properties

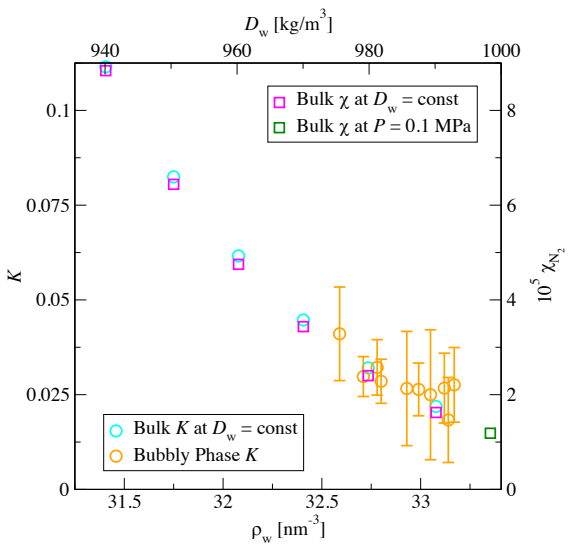

Figure 1: Partition coefficient and solubility for nitrogen between vapor and liquid phases or regions as functions of water number density. Data for bulk phases are obtained from Gibbs ensemble Monte Carlo simulations at T = 298 K, a nitrogen vapor pressure of 0.1 MPa, and either equilibrium (green square) or fixed (magenta squares) water densities. Data for the bubbly phase are obtained from canonical ensemble molecular dynamics simulations at T = 298 K and a nitrogen mole fraction of 1.0 × 10^{-3}.

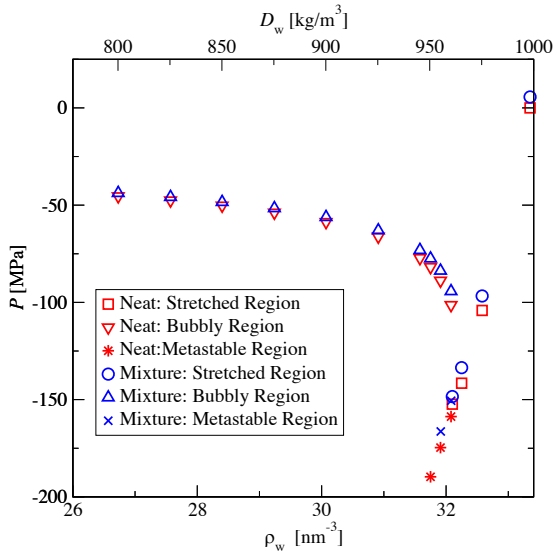

Figure 2: System pressure versus density for neat water (red symbols) and the water/nitrogen mixture (blue symbols) at T = 298 K. Squares and circles represent homogeneously stretched and bubbly water systems, respectively. The stars and crosses show data for metastable homogeneously stretched systems. Uncertainties are all smaller than the symbol size. With the exception of the value at D_w = 960.32 kg/m3, the data for neat water are taken from Chen, *et al.* (2019).

by the presence of nitrogen is only very minor. The data shown in Figure 1 demonstrate that the nitrogen solubility, in terms of mole fraction, increases by a factor of 7.3 as water is stretched from the equilibrium density to 940 kg/m^3. The increases in the nitrogen mole fraction and the corresponding vapor-liquid partition coefficient (determined from the ratio of nitrogen number densities in the liquid and vapor phases) are found to be slightly stronger than linear. The thermodynamic reason for the increase in solubility is the reduction of the entropic cost of solvation due to a larger number and larger size of transient voids in water under tension, i.e., it is easier to find a cavity to accommodate a nitrogen molecule as the water density is decreased.

Effects of Nitrogen on Thermophysical Properties

The system pressure (calculated here from the intermolecular forces) is one of the most important properties for homogeneously stretched and bubbly systems. As mentioned above, a nitrogen mole fraction of about 10^{-3} (80 times higher than the equilibrium mole fraction at P = 0.1 MPa) was used for the current simulations. As can be seen from Figure 2, the presence of nitrogen leads to a slight upward shift in the pressure for all water densities investigated here. Again, the systems exhibit a homogenously stretched region, where the pressure decreases approximately linearly with decreasing water density. The homogeneously stretched region ends at the spinodal point. Whereas a metastable stretched phase is still observed for neat water with a specific density of 950 kg/m^3 (Chen, *et al.*, 2019), the lowest density for the water/nitrogen mixture is D_w = 955 kg/m^3. That is, the barrier for nucleation is reduced and, hence, the homogeneously stretched phase is less stable.

In the bubbly region, the pressure decreases with increasing ρ_w for both neat water and the water/nitrogen mixture due to the decreasing size of the bubble (Chen, *et al.*, 2019). Here, the presence of nitrogen shifts the pressure upward (i.e., to less negative values and the increase is smallest at the lowest ρ_w, where the bubble volume is largest.

As the binodal point is approached, the absolute and relative shifts in pressure due to the presence of nitrogen become more pronounced. For both neat water and the water/nitrogen mixture, a

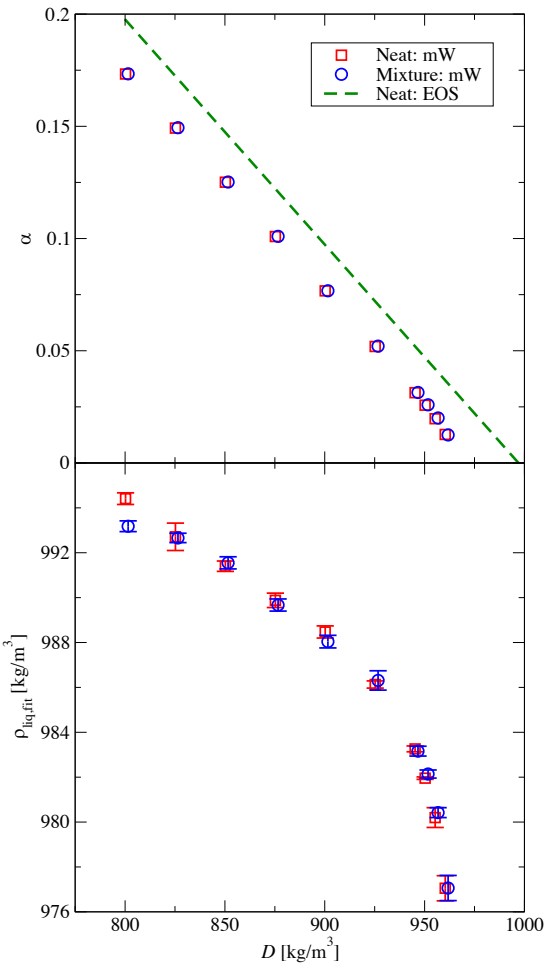

Figure 3: Bubble volume fraction (α) (top) and specific density in the liquid region ($\rho_{liq,fit}$) (bottom) versus system density for neat water (red symbols) and the water/nitrogen mixture (blue symbols) at T = 298 K. The green dashed line represents the analytic equation $\rho = (1 - \alpha)\rho_{liq} + \alpha\rho_{vap}$, where ρ_{liq} and ρ_{vap} are taken from experiment. The statistical uncertainties are only shown when larger than the symbol size. The data for neat water are taken from Chen, *et al.* (2019).

stable bubble is observed at D_w = 960.32 kg/m^3, but a slight increase to D_w = 960.97 kg/m^3 leads to a homogeneously stretched phase, i.e., a shift in the binodal point is not observed.

For the bubbly systems, Figure 3 illustrates the behavior of the bubble volume fraction and of the specific density of the liquid region as function of the system density (i.e., the sum of the water and nitrogen densities for the water/nitrogen mixture). The bubble volume fractions are very slightly larger for the water/nitrogen mixture than for neat water, but this effect is mostly due to the shift in the system density. At first glance, this might appear surprising because the presence of some solvated nitrogen molecules should lead to a swelling of the liquid region. The vapor-liquid distribution coefficients for nitrogen in the bubbly systems (calculated from the radial density profiles) are in good agreement with the bulk partition coefficients, but those for the inhomogeneous system suffer from large statistical uncertainties (see Figure 1). At D = 960 kg/m^3, the volume of the liquid region is about 80 times larger than the bubble volume, and the distribution coefficient is about 0.04. Thus, about 12 nitrogen molecules are present in the liquid region at this condition. The number of nitrogen molecules in the liquid region decreases further with increasing bubble volume fraction. Nevertheless, the presence of these nitrogen molecules in the liquid region does not lead to a net increase in the volume of the liquid region, because the system pressure is less negative, i.e., the liquid region is under less tension for the mixture than the neat water system. Comparison of the specific densities in the liquid region from radial density profiles does not yield a systematic shift between neat water and the mixture (see Figure 3).

For the bubbly region, the negative of the system pressure P is plotted against the reciprocal of the bubble radius r^* in Figure 4. The correlation between $-P$ and $1/r^*$ is close to linear for both neat water and the water/nitrogen mixture. However, for a given bubble radius, P is larger in magnitude for neat water, and this difference increases with decreasing bubble radius. Therefore, we can conclude that even at the sub-3 nm scale, the Young-Laplace equation is still applicable within some small tolerance. When the surface tension value γ^* is estimated by applying the Young-Laplace equation to each individual data point, then a trend emerges where γ^* increases nearly linearly with decreasing inverse bubble radius for both neat water and the water/nitrogen mixture (see Figure 4). Thus, formation of the convex liquid-vapor surface results in a smaller free energy penalty than for the planar surface. The slope of γ^* versus $1/r^*$, a metric for the curvature effect, is more negative for the mixture than for neat water. The larger curvature effect and lower γ^* values for the mixture explain why its nucleation barrier is smaller and it cannot sustain the same maximum tension before cavitation becomes spontaneous. Recently, Liu & Cao (2016) carried out molecular dynamics simulations for water nanodroplets with radii ranging from 1.3 to 2.7 nm and also found the Young-Laplace equation to hold well. In contrast to our work on nanobubbles, Liu & Cao did not observe any systematic shift in the surface with droplet radius. Given the well-known asymmetry of hydrogen-bonding at the liquid-vapor interface (Kuo, *et al.*, 2006), the curvature at the

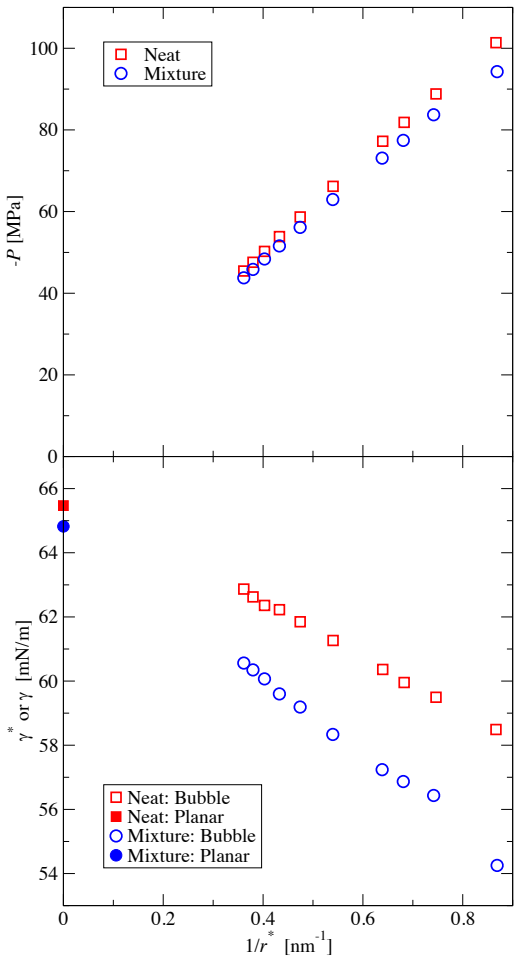

Figure 4: Negative system pressure (top) and bubble surface tension (bottom) versus inverse bubble radius for neat water (red symbols) and the water/nitrogen mixture (blue symbols) at T = 298 K. The statistical uncertainties are smaller than the symbol size. The data for neat water are taken from Chen, *et al.* (2019).

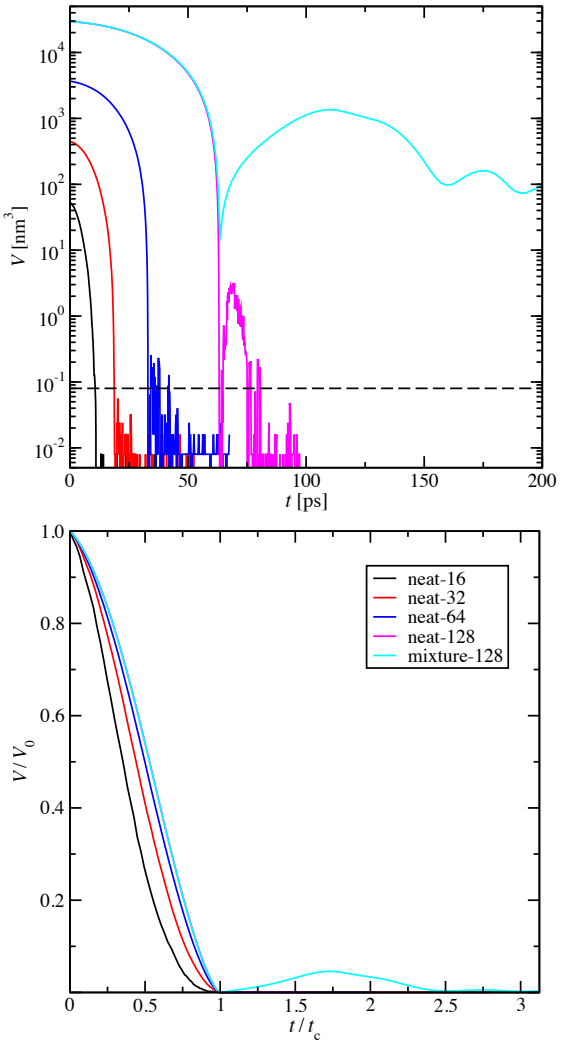

Figure 5: Time evolution of the bubble volume for neat water (L = 16, 32, 64, and 128 nm) and the water/nitrogen mixture. The top part represents the data in absolute units with the horizontal dashed line indicating the bubble-void cut-off. The data in the bottom part are normalized by initial bubble volume and collapse time.

bubble surface may allow for a small increase in the coordination number and, hence, a reduction in the surface tension.

Bubble Collapse: Effects of Nitrogen

The time evolutions for the bubble volume, V, for neat water with four different system sizes and the water/nitrogen mixture are illustrated in Figure 5. For larger system sizes, the initial bubble volume is larger and the time taken for the bubble collapse becomes longer. Due to the existence of transient voids even in single-phase liquid water, a cut-off is needed to distinguish between bubbles and voids. Here, a value of 0.08 nm^3 (i.e., 10 voxels) is used. This value is approximately three times larger than the molecular volume of a water molecule in the liquid phase and significantly larger than the size of transient voids found previously in homogeneous systems (Chen, *et al.*, 2019). The bubble collapse point is defined as the time where the bubble volume decays below this cut-off for the neat water systems and as the first volume minimum for the water/nitrogen mixture. For neat water, the largest system exhibits qualitatively different behavior from the three smaller systems. A clear rebound after initial collapse is observed only for the largest system (L = 128 nm). During the

rebound, a new bubble emerges, reaches a volume of more than 3 nm^3, and persists for about 10 ps until it disappears. For the second largest system (L = 64 nm), there is an emergent rebound, but the new bubble does not grow beyond 0.3 nm^3 (i.e., about the volume of 10 water molecules) and oscillates around the bubble threshold for about 8 ps before disappearing. Comparing the time evolutions in relative units (normalized by bubble collapse time and initial bubble volume, bottom part of Figure 5), then it is also evident that the evolutions for the two larger systems are very close (the maximum non-dimensionalized vertical deviation is 0.04), whereas the evolutions are significantly shifted for the smaller systems (with maximum vertical deviations of 0.28 and 0.13 for L = 16 and 32 nm, respectively, compared to L = 128 nm). Thus, subsequent discussion focuses entirely on the largest system size that was also used for the water/nitrogen mixture.

Already from the evolution of the bubble volume is it clear (see Figure 5), that there are marked differences near the initial collapse point and thereafter when nitrogen is present in the initial bubble. For the first 50 ps, the bubble volume evolutions are very similar. Beyond this, the collapse is slightly slowed down for the water/nitrogen mixture, but the collapse point is only delayed by 0.4 ps (from 63.2 to 63.6 ps). More importantly, at the first minimum, the bubble volume remains above 15 nm^3 for the mixture, i.e., the bubble does not actually collapse completely. During the first rebound, the bubble grows back to a volume of 1400 nm^3 (about 5% of its initial volume). After this first rebound, the bubble volume decreases again, but less violently, and the volume at the second minimum is 97 nm^3. The subsequent oscillation yields a volume minimum of 73 nm^3. The more pronounced rebound and the slow decay of the minimum volume during subsequent oscillation provide preliminary indication that the initial collapse does not lead to dissolution of a significant fraction of nitrogen molecules.

Figures 6-8 provide microscopic-level information on local density, temperature, and momentum in the vicinity of the initial bubble collapse point. At $t^* = t - t_c = -0.5$ ps (just before the collapse point), the volumes (radii) of the vapor and gas bubbles are 32 and 44 nm^3 (2.0 and 2.2 nm), respectively. The reason for slightly smaller size of the vapor bubble is that the collapse is more violent, i.e., the rate at which the bubble radius decays is larger for the vapor bubble than the gas bubble (see below). The water densities in the liquid region and bubble regions are close to the equilibrium values of 998 and $\approx$ 0 kg/m^3, respectively, for both the vapor and gas bubble collapse. At the collapse point, the local water density exceeds 1500 kg/m^3 for the vapor bubble collapse. In contrast, for the gas bubble collapse, the water density in the center of the bubble remains close to $\approx$ 0 kg/m^3, but there is a sphere of high-density water with 1300 kg/m^3 at a radius slightly larger than the bubble radius, i.e., there is incomplete mixing for the water/nitrogen mixture. After the bubble collapse point, a more pronounced density wave is observed for neat water than for the mixture. At $t^* = -0.5$ ps, the nitrogen in the outer region of the bubble (near the bubble wall) is compressed to a density 500 times larger than the equilibrium gas density (see Figure 7). At the bubble collapse point, the nitrogen reaches a density peak about 1000 times greater than the equilibrium density. The nitrogen density in the bubble remains very high during the rebound.

The lack of a high-density shell for water near the bubble surface during the collapse process indicates that, despite the rapid decrease in interfacial area, the interfacial water molecules are incorporated into the growing liquid region almost instantaneously. In contrast, the dissolution process for the nitrogen molecules proceeds much slower than the bubble collapse process, and about 90% of the nitrogen molecules are found in the rebounding bubble after the initial collapse. Similarly, very few water molecules get incorporated into the gas bubble during rebound, but the liquid-gas interface becomes less sharp. The difference in these time scales explains why the gas bubble collapse is less violent, the bubble does not vanish completely during the initial collapse, and the rebound with subsequent oscillations is much more pronounced for the gas bubble than the vapor bubble.

Figures 6 and 7 also show data for the local temperature (averaged over voxels with a 1 nm edge length). Again, there are interesting differences between the vapor and gas bubble collapse processes. At $t^* = -0.5$ ps, the highest temperature is observed for water molecules at the bubble surface for the vapor bubble. In contrast, for the gas bubble, the highest temperature is observed for a shell of nitrogen molecules just inside of the bubble surface, where the nitrogen molecules are highly compressed. These nitrogen molecules reach higher temperatures than those found for the water molecules in the neat water system. At the collapse point, the hot spot is highly localized at the bubble origin for both the vapor and gas bubbles. Actually, for the gas bubble collapse, these snapshots indicate a slightly higher temperature being reached at $t^* = -0.25$ ps. During the initial rebound of the vapor bubbles, the highest temperatures are still localized at the bubble origin despite the strong density wave having moved away.

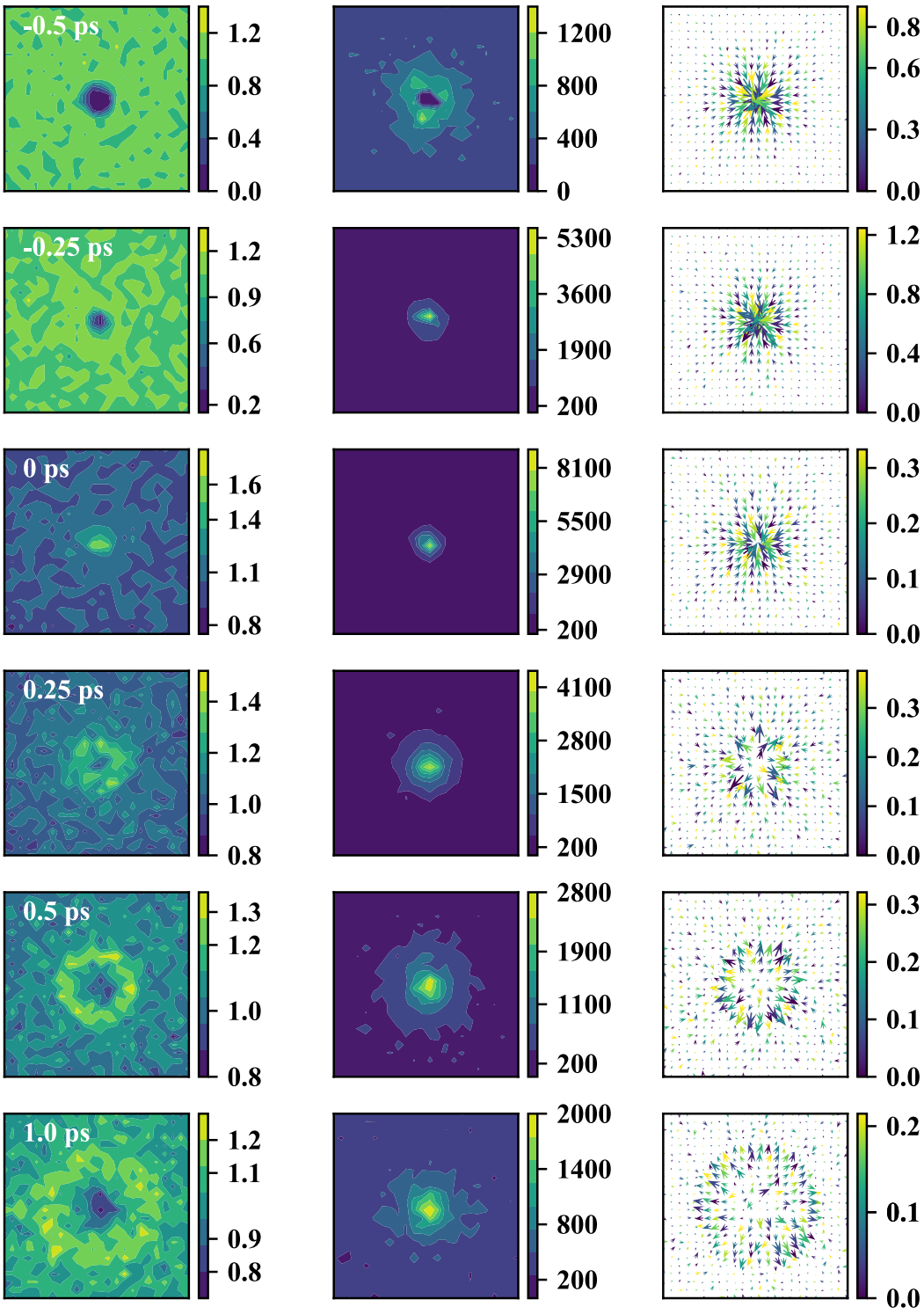

Figure 6: Cross-sectional heat maps for the vapor bubble collapse showing the central 24 ×24 nm^2 region of the simulation box with properties computed on a 1 × 1 nm^2 mesh: (Left) Water number density normalized by the liquid density at T = 298 K and P = 1 bar; (Middle) Kinetic temperature in units of kelvin; (Right) Voxel velocity normalized by the speed of sound for neat liquid water at T = 298 K and D_w = 998 kg/m^3.

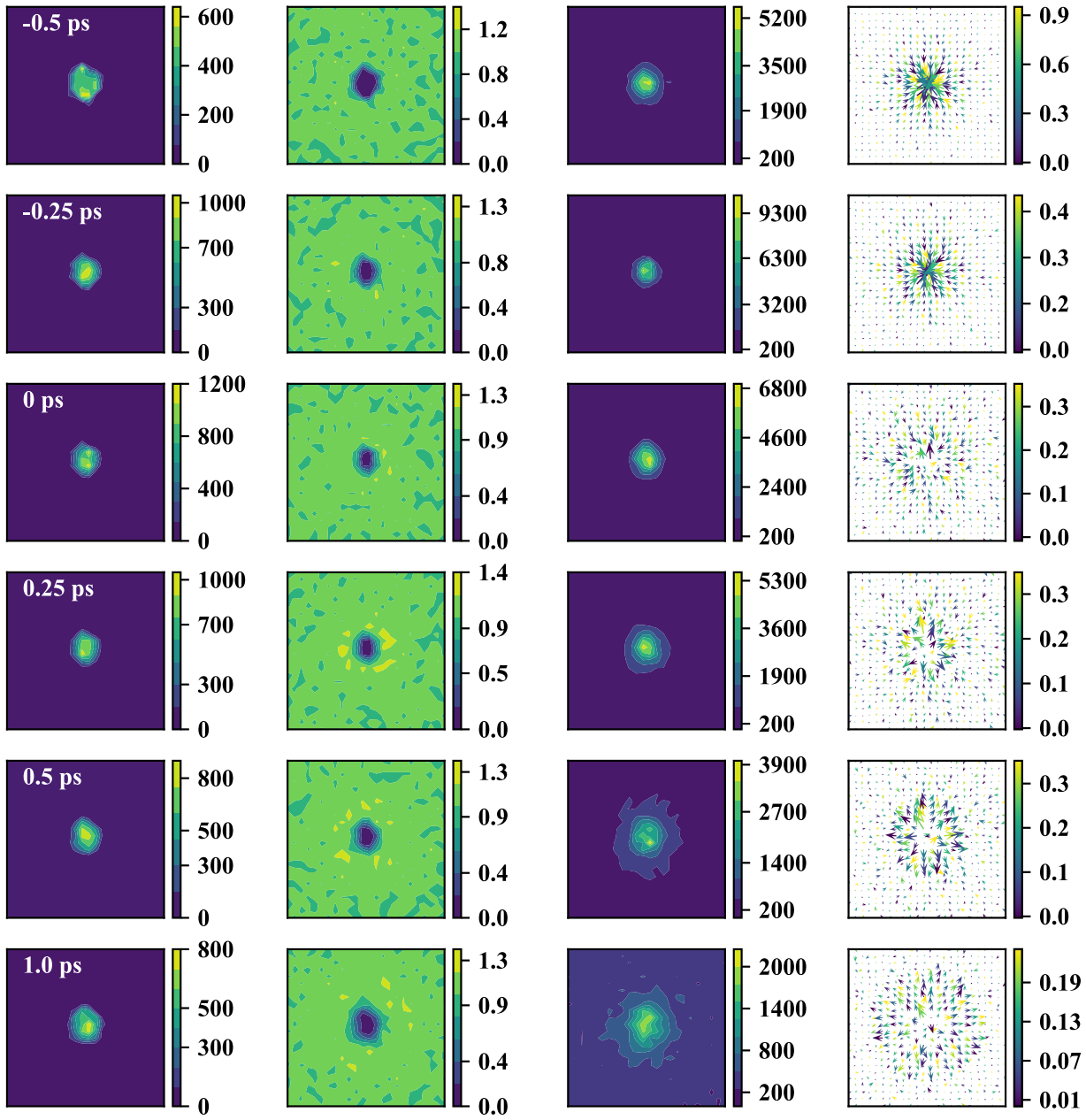

Figure 7: Cross-sectional heat maps for the as bubble collapse showing the central 24 ×24 nm^2 region of the simulation box with properties computed on a 1 × 1 nm^2 mesh: (Left) Nitrogen number density normalized by the vapor density at T = 298 K and P = 1 bar; (Left middle) Water number density normalized by the liquid density at T = 298 K and P = 1 bar; (Right middle) Kinetic temperature in units of kelvin; (Right) Voxel velocity normalized by the speed of sound for neat liquid water at T = 298 K and D_w = 998 kg/m^3.

Summing the velocity vectors in a given voxel yields information on the local mass transport. At t^* = −0.5 and −0.25 ps, there are strong mass waves moving toward the bubble origin for both the vapor and gas bubbles. Although the qualitative features are similar, this mass wave reaches much higher speeds for the vapor bubble than for the gas bubble. Here the voxel velocities are normalized by the speed of sound of the mW model that is 2281 ± 58 m/s as calculated from a separate simulation in the canonical ensemble at T = 298 K and D_w = 998 kg/m^3. Overall, the cross-sectional heat maps indicate a less violent collapse and a softer rebound process for the gas bubble compared to the vapor bubble; this is supported by radial analysis (see below).

Figure 8 shows a molecular representation of the gas bubble collapse. Specifically, approximately 2000 molecules closest to the bubble origin are selected. Remember that the system contains 832 nitrogen molecules, so the 2000 molecules provide a good representation of interfacial water molecules without completely obscuring the bubble interior. At t / t_c = 0.9, the density of nitrogen in the bubble exceeds the equilibrium gas density by a factor of 20. At the collapse point, the nitrogen is compressed by an additional factor of 50, i.e., the nitrogen density reaches a liquid-like number density of more than 20 molecules per nm^3. This high compression is also evident from the bottom snapshot, where the nearest-neighbor distance between two nitrogen molecules becomes similar to that for two water molecules.

All four snapshots also indicate the limited extent of mixing. Water molecules do not enter the interior of the bubble to any significant extent. The decrease in bubble volume and surface area results in a higher coverage of the surface for these 2000-molecule snapshots. The water surface appears patchy at $t / t_c \leq 0.98$ because the bubble is not exactly spherically symmetric. However, since no water multi-layers are observed, variations in the local distance of the surface from the bubble center are quite small.

Given that the shape anisotropy is very small even for sub-3 nm bubbles (Chen, *et al.*, 2019), the bubble dynamics can be quantified by the evolution of the bubble radius and the corresponding time derivative, called here the wall velocity (see Figure 9). As already deduced from the time evolution of the bubble volume, the initial trajectories are remarkably similar for the vapor and gas bubble collapses. However, as the nitrogen gets highly compressed in the later stages of the gas bubble collapse, the wall velocity for the water/nitrogen mixture does not accelerate to the same extent as for

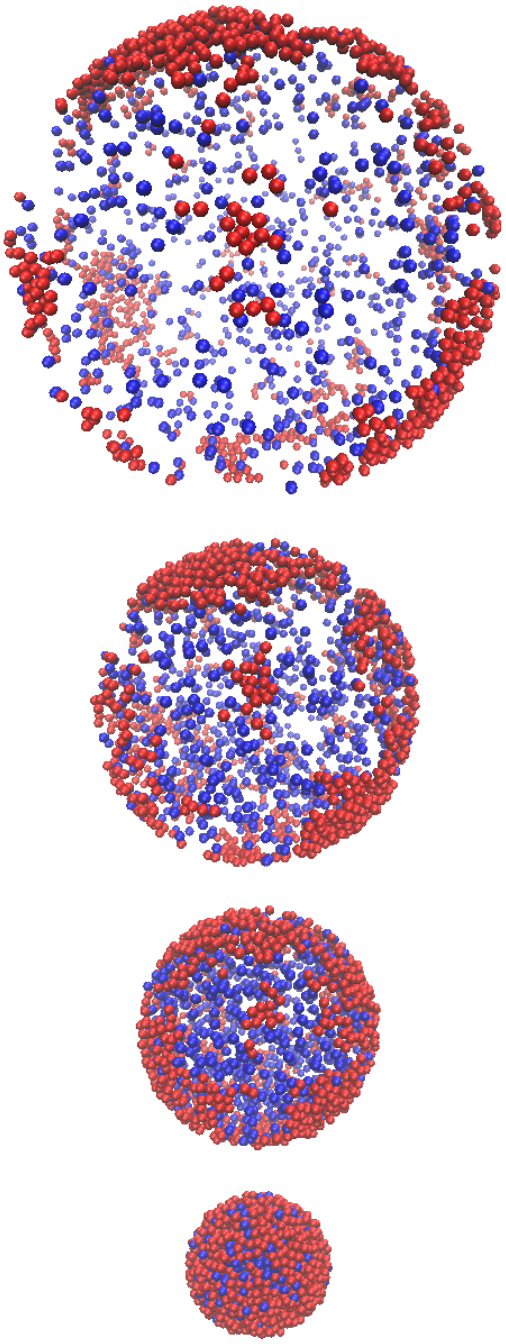

Figure 8: Snapshots of the bubble surface and interior for the water/nitrogen mixture at t / t_c = 0.9, 0.95, 0.98, and 1.0 (top to bottom). A total of approximately 2000 molecules is shown; the water and nitrogen molecules are depicted as red and blue spheres, respectively. The corresponding bubble radii are 7.2, 4.8, 3.2, and 1.5 nm, respectively; and the 2000-molecule radii are 7.2, 4.9, 3.5, 2.4 nm, respectively.

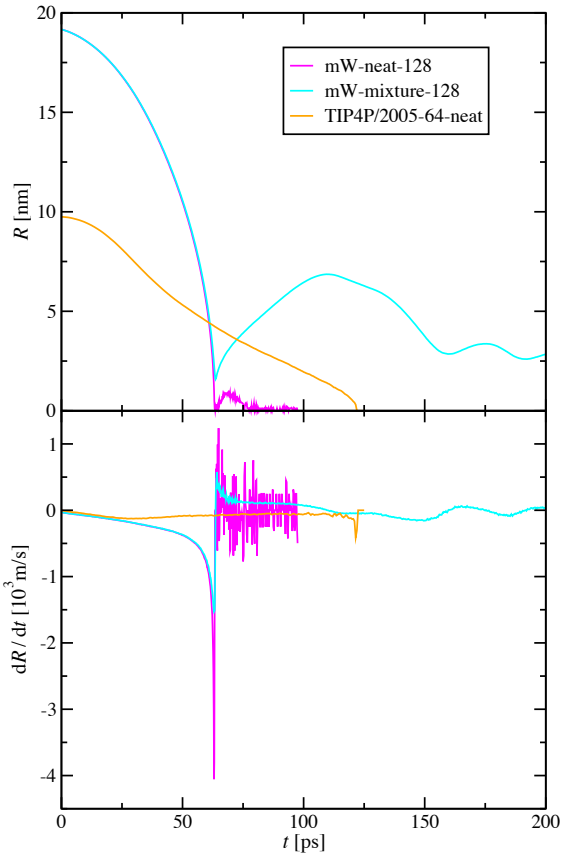

Figure 9: Time evolution of the bubble radius (top) and of the wall velocity (bottom) for vapor and gas bubbles with the mW model and for the vapor bubble with the TIP4P/2005 model.

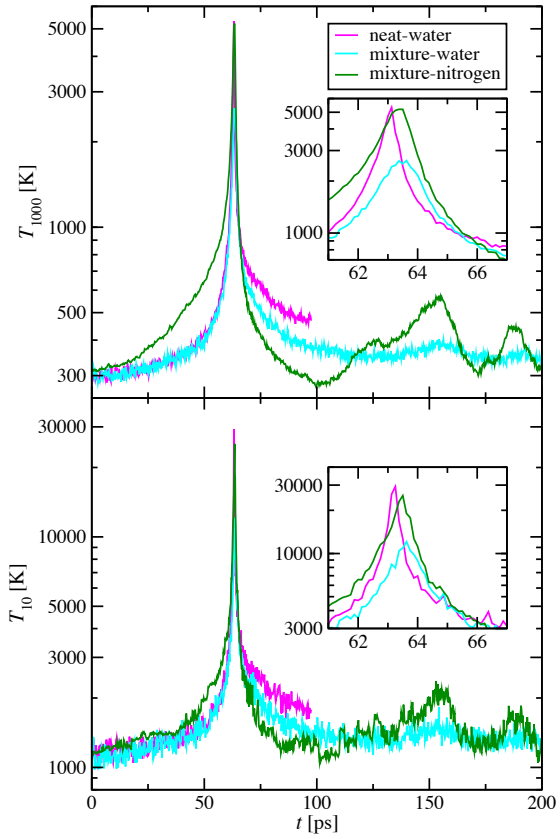

Figure 10: Time evolution of the temperature in the innermost shell averaged over ≈1000 molecules (top) and of the threshold temperature for the top 1% of molecules in this innermost shell (bottom). For the gas bubble, the temperatures are calculated separately for the water and nitrogen molecules.

the vapor bubble. For both vapor and gas bubbles, the maximum wall velocity is reached at t = 63 ps, and the maximum wall velocity for the vapor bubble exceeds that for the gas bubble by a factor of 2.6.

During rebound, the maximum positive velocity for the gas bubble is observed 0.5 ps after collapse. The small oscillations evident in the wall velocity of the gas bubble during the first rebound are caused by interferences/reflections of the originally outward traveling density waves in our periodic system. Due to the very small size of the vapor bubble during rebound, the wall velocity shows large fluctuations.

To provide more quantitative information on the temperature evolution, the system is divided into spherical shells of approximately 1000 molecules. The highest temperature is almost always found for the innermost shell. Hence, the evolution of the instantaneous temperature averaged over the ≈1000 molecules in this shell is presented in Figure 10. The time evolution of the temperatures for the water molecules are remarkably similar for the vapor and gas bubble collapse. The driving force for the bubble collapse is the reduction of the system pressure and the surface area. Reducing the bubble size allows more water molecules to be incorporated into the liquid phase which leads to a decrease in the potential energy for the water molecules and a corresponding increase in the kinetic energy. At the collapse point, the innermost 1000-molecule shell temperature for water exceeds 5000 and 2500 K for the vapor and gas bubbles, respectively. Instead of averaging over ≈1000 molecules, it is also instructive to analyze the threshold temperature for the top-1% of molecules in this shell because these molecules are most likely to cause materials damage and cavitation erosion. For the vapor bubble, the threshold temperature reaches nearly 30000 K. A similar threshold temperature is also reached for the nitrogen molecules in the gas bubble, whereas that for the water molecules is lower

by a factor of 2. Extreme temperatures above 10^4 K were also observed in previous hybrid Rayleigh-Plesset molecular-dynamics simulations [Bass, *et al*., 2008; Schanz, *et al.*, 2012].

A significant difference for the water and nitrogen molecules is also observed during much of the gas bubble collapse. At t = 50 ps (t/t_c = 0.8), the nitrogen/water temperature ratio in the innermost shell reaches 1.6 and remains close to this value until the collapse point. During the rebound, this pattern is reversed; presumably because the nitrogen molecules experience more expansion cooling. This pattern is repeated during the subsequent oscillations in bubble size.

Up to this point, the discussion has focused on simulations for the computationally efficient mW water model. Figure 9 also presents the evolution of the bubble radius and wall velocity for the vapor bubble collapse obtained from a simulation with the atomistic TIP4P/2005 water model. Even considering the difference in system size and initial bubble radius, the differences between the two models are striking. The collapse time for the TIP4P/2005 water model exceeds those obtained with the mW water model for the same and twice the initial radius by factors of 4 and 2, respectively. More importantly, whereas the magnitude of the wall velocity for the mW model monotonically increases for $t/t_c < 0.99$, it reaches a maximum at $t/t_c = 0.23$ for the TIP4P/2005 model. Thereafter, it slows significantly and only accelerates for $t/t_c > 0.95$, when the bubble radius reaches 1.1 nm, i.e., close to the smallest stable bubble observed in prior equilibrium simulations [Chen, *et al*., 2019].

In an effort to validate the numerical results from these simulations and to explain the striking differences between the data for the mW and TIP4P/2005 models, we compare the time evolution of the bubble radius for these models to numerical solutions for the Rayleigh and Rayleigh-Plesset equations [Rayleigh, 1917; Plesset & Prosperetti, 1977; Franc & Michel, 2005]. To this extent, the Rayleigh equation is solved either using a constant pressure (where the average value during collapse is used, and the equation becomes essentially identical to the analytical form developed by Obreschkow *et al*. [2012]) or using the instantaneous value of the pressure from the molecular simulations. For the Rayleigh-Plesset equation, the instantaneous pressure is used, but the kinematic viscosity and surface tension are taken as constant and are those reported previously for the mW and TIP4P/2005 models for the saturated liquid phase at T = 298 K [Chen, et al., 2019]. As can be seen from Figure 11, using the instantaneous pressure reduces the collapse time predicted by the Rayleigh equation by about 15-20%.

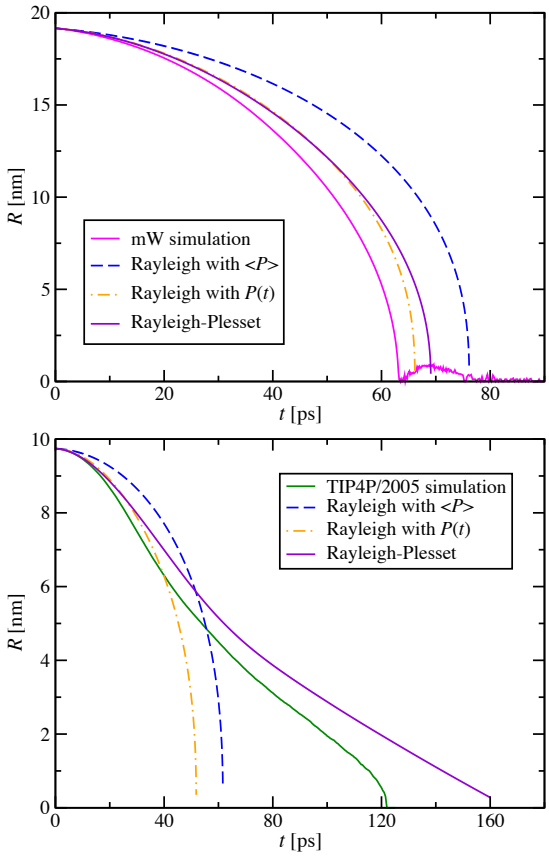

Figure 11: Comparison of the time evolutions of the bubble radius for the mW model (top) and TIP4P/2005 model (bottom) with numerical solutions of the Rayleigh equation using the average value of the pressure from the simulation, the Rayleigh equation using the instantaneous value of the pressure from the simulation, and the Rayleigh-Plesset equation.

For the mW model, the Rayleigh-Plesset equation yields a collapse time that is about 5% larger than the Rayleigh equation with instantaneous pressure. The molecular dynamics simulation for the mW model yield a collapse time that is 10% less than the Rayleigh-Plesset equation. Nevertheless, the evolution of the bubble radius is in good qualitative agreement for the simulations and the three macroscopic equations.

In contrast, qualitative differences are found for the TIP4P/2005 water model. Here, the Rayleigh equation shows a monotonic increase in the magnitude of the wall velocity and underpredicts the collapse time by more than a factor of 2 compared to the molecular dynamics simulations. On the other hand, the Rayleigh-Plesset equation yields the correct shape, but over predicts the collapse time by 30%.

These observations indicate that the molecular dynamics simulations yield bubble evolutions that are consistent with the Rayleigh-Plesset equation for both the mW and TIP4P/2005 models, but that the qualitative differences between the models are due to differences in their thermophysical properties. Our prior simulations show that both models yield the same equilibrium surface tension (that is about 10% lower than the experimental value), but that only the TIP4P/model yields an accurate viscosity, whereas the mW model yields an underestimation by nearly a factor of 3 [Chen, *et al.*, 2019].

CONCLUSIONS

The molecular simulations presented here provide a wealth of information on the effects of nitrogen on the thermophysical properties of homogeneously stretched and bubbly water and on the bubble collapse dynamics. Considering first equilibrium properties, addition of nitrogen at an 80-times higher concentration than the equilibrium nitrogen mole fraction at P = 1 bar is found to yield no dramatic changes in system pressure, locations of spinodal and binodal points, bubble volume fraction, and surface tension. Although the current simulations consider only a relatively small system with L = 8 nm (14000 – 17000 water molecules), it is likely that these observations will also hold on the micrometer scale when the nitrogen mole fraction is reduced to the equilibrium mole fraction of 1.2×10^{-5}. At this very low concentration, the entropic penalty for aggregation of nitrogen molecules is hard to overcome. The simulations also indicate an increase in the nitrogen solubility for water under tension due to an increase in transient molecular-sized cavities.

In contrast, even at the equilibrium mole fraction of 1.2×10^{-5}, the presence of nitrogen qualitatively changes the bubble collapse dynamics. The reason is that dissolution of nitrogen occurs on a much slower time scale than the bubble collapse and rebound. During the collapse process, significant mixing does not occur and the nitrogen molecules in the interior of the bubble are compressed to liquid-like densities. This nitrogen "droplet" prevents the complete collapse of the bubble (when the bubble volume is detected based on the local regions not occupied by water molecules). Near the collapse point, the wall velocity for the vapor bubble exceeds the bulk-liquid-phase speed of sound and is 2.6 times larger than that for the gas bubble.

Bubble collapse simulations with the coarse-grained mW and atomistic TIP4P/2005 model yield qualitatively different time evolutions. Comparison to numerical solution of the Rayleigh-Plesset equation are consistent with the simulation data for both models and show that the underprediction of the viscosity by the mW model is responsible for the different behavior compared to the TIP4P/2005 model.

In future work, the simulations of collapse dynamics will be extended to even larger system sizes and a smaller R_I / L ratio for the mW water model and to water/nitrogen mixtures for the TIP4P/2005 water model.

ACKNOWLEDGEMENTS

This work is supported by the United States Office of Naval Research under Grant ONR N00014-17-1-2676 with Dr. Ki-Han Kim as the program manager. Part of the computer resources was provided by the Minnesota Supercomputing Institute.

REFERENCES

Abascal, J.L.F. and Vega, C., "A general purpose model for the condensed phases of water: TIP4P/2005. Journal of Chemical Physics, Vol. 123, No. 23, article no. 234505.

Bass, A., Ruuth, S. J., Camara, C., Merriman, B., and Putterman, S., "Molecular dynamics of extreme mass segregation in a rapidly collapsing bubble," Physical Review Letters, Vol. 101, No. 23, 2008, article no. 23401.

Chapoy, A., Mohammadi, A.H., Tohidi, B., and Richon, D., "Gas Solubility Measurement and Modeling for the Nitrogen + Water System from 274.18 K to 363.02 K," Journal of Chemical and Engineering Data, Vol. 49, No. 6, 2004, pp. 1110-1115.

Chen, J.L., Xue, B., Mahesh, K., and Siepmann, J.I., "Molecular Simulations Probing the Thermophysical Properties of Homogeneously Stretched and Bubbly Water Systems," Journal of Chemical and Engineering Data, Vol. 64, No. 9, 2019, pp. 3755-3771.

Crowe, C.T. Multiphase Flow Handbook, CRC Press, Boca Raton, 2005.

Franc, J.-P. and Michel, J.M. Fundamentals of Cavitation, Fluid Mechanics and Its Applications, Vol. 76, 2005.

Holyst, R., Litniewski, M., and Garstecki, P., "Large-scale molecular dynamics verification of the Rayleigh-Plesset approximation for collapse of

nanobubbles," Physical Review E, Vol. 82, 2010, article no. 066309.

Japas, M.L. and Franck, E.U., "High Presssure Phase Equilibria and PVT-Data of the Water-Nitrogen System to 673 K and 250 MPa," Berichte der Bunsengesellschaft für Physikalische Chemie, Vol. 6, No. 7, 1985, pp. 793-800.

Kuo, I-F.W., Mundy, C.J., Eggimann, B.L., McGrath, M.J., Siepmann, J.I., Chen, B., Vieceli, J., and Tobias, D.J., "Structure and Dynamics of the Aqueous Liquid-Vapor Interface: A Comprehensive Particle-Based Simulation Study," Journal of Physical Chemistry B, Vol. 110, No. 8, pp. 3738-3746.

Liu, H. and Cao, G., "Effectiveness of the Young-Laplace equation at nanoscale," Scientific Reports, Vol. 6, 2016, article no. 23936.

Matsumoto, M., Miyamoto, K., Ohguchi, K., and Kinjo, T., "Molecular dynamics simulation of a collapsing bubble," Progress of Theoretical Physics Supplement, Vol. 138, 2000, pp. 728-729.

Molinero, V. and Moore, E.B., "Water modeled as an intermediate element between carbon and silicon," Journal of Physical Chemistry B, Vol. 113, No. 13, 2008, pp. 4008-4016.

Obreschkow, D., Bruderer, M. and Farhat, M., "Analytical approximations for the collapse of an empty spherical bubble," Physical Review E, Vol. 85, 2012, article no. 066303.

Panagiotopoulos, A.Z., Quirke, N., Stapleton, M., and Tildesley, D.J., "Phase equilibria by simulation in the Gibbs ensemble: Alternative derivation, generalization and application to mixture and membrane equilibria," Molecular Physics, Vol. 63, No. 4, 1988, pp. 527-545.

Plesset, M.S. and Prosperetti, A., "Bubble Dynamics and Cavitation," Annual Review of Fluid Mechanics, Vol. 9, 1977, pp. 145-185.

Rayleigh, Lord O.M., "VIII. One the Pressure developed in a Liquid during Collapse of a Spherical Cavity," Philosophical Magazine, Vol. 34, 1917, pp. 94-98.

Rettich, T.R., Battino, R., and Wilhelm, E. "Solubility of Gases in Liquids. XVI. Henry's Law Coefficients for Nitrogen in Water at 5 to 50 ºC," Journal of Solution Chemistry, Vol. 13, No. 5, 1984, pp. 335-348.

Schanz, D., Metten, B., Kurz, T., and Lauterborn, W., "Molecular dynamics simulations of cavitation bubble collapse and sonoluminescence," New Journal of Physics, Vol. 14, No. 11, 2012, article no. 113019.

Xiao, C., Heyes, D.M., and Powles, J.G., "The collapsing bubble in a liquid by molecular dynamics simulations," Molecular Physics, Vol. 100, No. 21, 2002, pp. 3451-3468.

Yadigaroglu, G. and Hewitt, G.F., Introduction to Multiphase Flow: Basic Concepts, Applications and Modelling, Springer, Cham, 2017.